Constraining the Interiors of Asteroids Through Close Encounters: Appendices

Jack T. Dinsmore[1] and Julien de Wit[2]

[1]Department of Physics, Massachusetts Institute of Technology
[2]Department of Earth, Atmospheric, and Planetary Science, Massachusetts Institute of Technology

August 26, 2022

APPENDIX A: TIDAL TORQUE & EQUATIONS OF MOTION

In this appendix, we derive the equations of motion used to simulate the asteroid encounter. In particular, we describe our coordinates (section A.1) for an encountering asteroid's position and orientation, and we parametrize its density distribution via its density moments (section A.2). Then we derive an arbitrary-order equation for tidal torque (section A.3) and write the equations of motion for the system (section A.4).

A.1 Coordinates

We make use of two frames of reference to model this system. One is the "inertial frame," with axes denoted by $\hat{\boldsymbol{X}}$, $\hat{\boldsymbol{Y}}$, $\hat{\boldsymbol{Z}}$ and origin placed at the central body's centre of mass. $\hat{\boldsymbol{X}}$ points from the central body to the asteroid perigee, and $\hat{\boldsymbol{Z}}$ points parallel to the orbit angular momentum. We assume that the mass distribution of the central body is known in this inertial frame.

Our second frame is the "body-fixed" frame, denoted by $\hat{\boldsymbol{x}}, \hat{\boldsymbol{y}}, \hat{\boldsymbol{z}}$. Each axis in this frame is aligned with a principal axis and rotates with the asteroid, with its origin at the asteroid's centre of mass. For definiteness, we define $\hat{\boldsymbol{z}}$ to be the principal axis with maximal MOI (this is the short axis mode, to use the vocabulary of Kaasalainen 2001). In general, we use capital letters to denote vectors in the inertial frame and lowercase vectors to denote vectors in the body-fixed frame.

The difference between the origins of the body-fixed and inertial frames is the position of the asteroid. We represent the relative orientations by $z-y-z$ Euler angles α, β, and γ, such that a matrix M rotating from the body-fixed to the inertial frame ($M\boldsymbol{r} = \boldsymbol{R}$) is given by

$$M = R_z(\alpha)R_y(\beta)R_z(\gamma). \tag{A.1}$$

Here, $R_i(\theta)$ is a rotation around the unit vector i by angle θ (figure A.1).

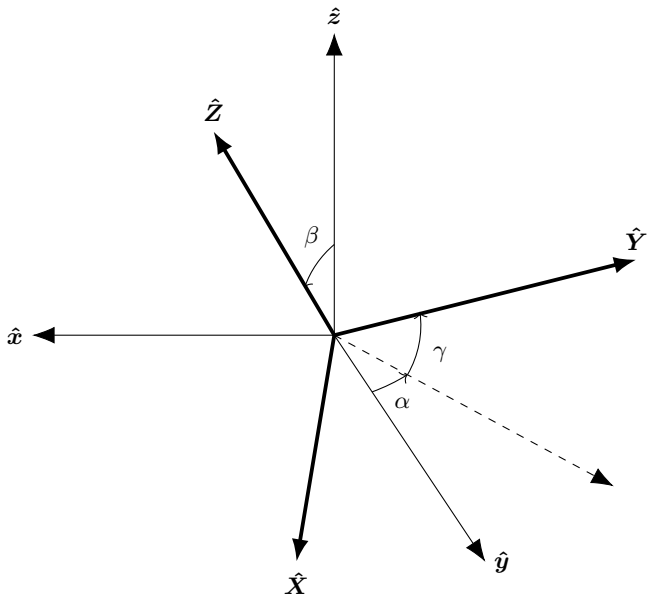

Figure A.1: $z-y-z$ Euler angles used in this work to express the orientation of the asteroid. Orientation is expressed as a rotation from the body-fixed axes (lowercase) to the inertial axes (bold lines and uppercase). The origins are co-located for demonstration purposes.

A.2 Density moments

The un-normalized spherical harmonics are defined as $Y_{\ell m}(\theta, \phi) = P_{\ell m}(\cos\theta)e^{im\phi}$, where $P_{\ell m}$ are the associated Legendre Polynomials without the Condon-Shortley phase. The regular and irregular spherical harmonics are further defined as

$$\begin{aligned} S_{\ell m}(\boldsymbol{r}) &= (-1)^m(\ell-m)!\frac{Y_{\ell m}(\hat{\boldsymbol{r}})}{r^{\ell+1}} \\ R_{\ell m}(\boldsymbol{r}) &= (-1)^m\frac{r^\ell}{(\ell+m)!}Y_{\ell m}(\hat{\boldsymbol{r}}). \end{aligned} \tag{A.2}$$

These spherical harmonics obey many useful identities summarized in Gelderen 1998, which are also useful for quantum mechanics. They were used to define the density moments in equation 1, which can be extended to the central body:

$$J_{\ell m} = \frac{a_{\mathcal{B}}^{2-\ell}}{I_{\mathcal{B}}}\int_{\mathcal{B}} d^3r\rho_{\mathcal{B}}(\boldsymbol{r})R_{\ell m}(\boldsymbol{r}) \tag{A.3}$$

By contrast, $J_{\ell m}$ should be computed in the inertial frame. The length scale $a_{\mathcal{B}}$ and MOI scale $I_{\mathcal{B}}$ can be defined similarly to $a_{\mathcal{A}}$ and $a_{\mathcal{B}}$ in equations 3 and 2, but they could also be set to any other scales of the same units, e.g. $a_{\mathcal{B}}$ equal to the central body radius and $I_{\mathcal{B}} = \mu_{\mathcal{B}}a_{\mathcal{B}}^2$, where $\mu_{\mathcal{B}}$ is the central body mass.

ℓ	$\Re K_{\ell 3}$	$\Im K_{\ell 3}$	$\Re K_{\ell 2}$	$\Im K_{\ell 2}$	$\Re K_{\ell 1}$	$\Im K_{\ell 1}$	$K_{\ell 0}$
0							-
1					x	y	z
2			-	x,y	y,z	x,z	-
3	x,z	y,z	z	x,y,z	x	y	z

Table A.1: Axes of mirror symmetry that imply zeroed density moments. For example, for mirror symmetries along $\hat{\boldsymbol{y}}$ or $\hat{\boldsymbol{z}}$, $\Im K_{32} = 0$. Mirror symmetry along $\hat{\boldsymbol{x}}$ means $\rho_{\mathcal{A}}(x, y, z) = \rho_{\mathcal{A}}(-x, y, z)$. Dashes indicate that none of the mirror symmetries zero the moment in question. Since $r^2 > 0$ for $r \neq 0$, no symmetries set $a_{\mathcal{A}} = 0$ either.

Note that both $J_{\ell m}$ and $K_{\ell m}$ are unitless. We call them "moments" because $R_{\ell m}(\boldsymbol{r})$ contains an r^ℓ dependence so that $K_{\ell m}$ is the ℓth density moment of the asteroid.

These moments share several key properties which we discuss before continuing. Firstly, for real mass density, properties of the spherical harmonics imply that $K_{\ell m} = (-1)^m K^*_{\ell,-m}$. Therefore, the set of $K_{\ell m}$ for $\ell < \ell_{\max}$ contains $\ell^2_{\max}$ degrees of freedom. However, some of these degrees of freedom are redundant with the choice of coordinates: $K_{1m} = 0$ since the body-fixed frame is centred on the asteroid centre of mass. Further calculation reveals that the alignment of the body-fixed frame with the asteroid principal axes also forces $K_{21} = 0$ and $\Im K_{22} = 0$. The only physical density moments for $\ell \leq 2$ are therefore K_{22}, K_{20}, and K_{00}. The first two are related to the MOI around each principal axis by equation 5, while $K_{00} = \mu_{\mathcal{A}} a^2_{\mathcal{A}}/I_{\mathcal{A}}$ will not be relevant to this study as it does not appear in equation 4.

The physical meaning of K_{22} and K_{20} can also be interpreted via a special case: if the asteroid is a uniform-density triaxial ellipsoid, the moments of inertia are simple to compute in terms of the semi-axis lengths and can be compared to those found in equation 5. This yields semi-axis lengths of

$$\begin{aligned} a &= \sqrt{\frac{5}{3}} a_{\mathcal{A}} \sqrt{1 - 2K_{20} + 12K_{22}} \\ b &= \sqrt{\frac{5}{3}} a_{\mathcal{A}} \sqrt{1 - 2K_{20} - 12K_{22}} \\ c &= \sqrt{\frac{5}{3}} a_{\mathcal{A}} \sqrt{1 + 4K_{20}}. \end{aligned} \tag{A.4}$$

The higher-order moments K_{3m} can be thought of loosely as measuring the large-scale asymmetries of the asteroid. An asteroid that is mirror-symmetric along the $\hat{\boldsymbol{x}}$ axis (meaning $\rho_{\mathcal{A}}(x, y, z) = \rho_{\mathcal{A}}(-x, y, z)$) necessarily sets certain density moments to zero. Which density moments are zeroed by which mirror symmetries is outlined in table A.1. All K_{3m} are zeroed by at least one mirror symmetry.

Finally, the requirement that $\rho_{\mathcal{A}}(\boldsymbol{r}) \geq 0$ everywhere restricts $K_{\ell m}$. In the case of K_{2m}, this fact and the constraint that I_z is larger than I_x or I_y requires K_{20} and K_{22} to fall in the triangle

$$-\frac{1}{4} \leq K_{20} \leq 0, \qquad |K_{22}| \leq \frac{|K_{20}|}{2}. \tag{A.5}$$

An analytical constraint on K_{3m} based on this property is more difficult to derive, but in practice, we observe that $|K_{3m}| < 0.01$.

A.3 Tidal torque

Derivations for the tidal torque experienced by a rigid body in the gravitational field of a larger mass have been computed by several previous studies (Paul 1988; Hou, Scheeres, and Xin Mar 2017; Boué and Laskar 2009; Ashenberg 2007), often in terms of the MOI of the rigid body (or higher order moments of inertia), and to varying degrees of precision. A simple, first-order derivation is also easily computable in terms of the asteroid MOI in the inertial frame.

Here, we present a new derivation of the tidal torque to arbitrary orders in terms of the density moments of an asteroid defined in section A.2. These density moments can be precomputed and do not have to be re-evaluated every time-step.

The gravitational potential energy of the central body is, in its most general form,

$$V(\boldsymbol{R}') = -G \int_{\mathcal{B}} d^3 R \frac{\rho_{\mathcal{B}}(\boldsymbol{R})}{|\boldsymbol{R} - \boldsymbol{R}'|}. \tag{A.6}$$

where $\rho_{\mathcal{B}}$ is the density distribution of the central body and $\mathcal{B}$ indicates the central body's volume. All vectors here are written in the inertial frame. Given $|\boldsymbol{R}| < |\boldsymbol{R}'|$, Gelderen 1998 gives the identity

$$\frac{1}{|\boldsymbol{R} - \boldsymbol{R}'|} = \sum_{\ell,m} R_{\ell m}(\boldsymbol{R}) S^*_{\ell m}(\boldsymbol{R}'), \tag{A.7}$$

where the sum is shorthand for $\sum_{\ell,m} = \sum_{\ell=0}^{\infty} \sum_{m=-\ell}^{\ell}$.

Incidentally, it is the $|\boldsymbol{R}| < |\boldsymbol{R}'|$ assumption that inspires the assumption that there are "no *distant* perturbing objects" (section 2). If a perturbing object such as a moon is not distant (i.e., it is closer to the system center of mass than the asteroid perigee so that $|\boldsymbol{R}| < |\boldsymbol{R}'|$ always), then it can be absorbed into $J_{\ell m}$ by equation A.3 and the assumptions of this derivation are not violated.

We are interested in translating the potential energy of equation A.6 to the body-fixed frame. To do this, we let $\boldsymbol{R}' = \boldsymbol{D} + \boldsymbol{U}$, where $\boldsymbol{D}$ is the location of the asteroid in the inertial frame. We further define $\boldsymbol{U} = M\boldsymbol{u}$, where $\boldsymbol{u}$ is in the body-fixed frame and M is the rotation matrix given by the Euler angles α, β, and γ (see section A.1). The translation from $\boldsymbol{R}'$ to $\boldsymbol{U}$ is then attained by the identity

$$S_{\ell m}(\boldsymbol{R}') = \sum_{\ell',m'} (-1)^{\ell'} R^*_{\ell' m'}(\boldsymbol{U}) S_{\ell+\ell', m+m'}(\boldsymbol{D}), \tag{A.8}$$

provided by Gelderen 1998, and from $\boldsymbol{U}$ to $\boldsymbol{u}$ is given by

$$\begin{aligned} Y_{\ell m}(M\boldsymbol{u}) = \sum_{m'=-\ell}^{\ell} (-1)^{m+m'} \sqrt{\frac{(\ell - m')!(\ell + m)!}{(\ell + m')!(\ell - m)!}} \\ \times \mathcal{D}^{\ell}_{mm'}(M)^* Y_{\ell m'}(\boldsymbol{u}). \end{aligned} \tag{A.9}$$

Here, $\mathcal{D}^{\ell}_{mm'}(M)$ are the Wigner-D matrices, which are determined by the Euler angles α, β, and γ of M.

Equations A.6 to A.9 then provide formula for $V(\boldsymbol{u})$ expressed as a sum of integrals over $\mathcal{B}$ of the central body density $\rho_{\mathcal{B}}(\boldsymbol{R})$ times $R_{\ell m}(\boldsymbol{R})$. These are expressed via equation A.3 as $J_{\ell m}$.

The tidal torque experienced by the asteroid (in the body-fixed frame) is given by

$$\boldsymbol{\tau}(\boldsymbol{u}) = \int_{\mathcal{A}} d^3 u \rho_{\mathcal{A}}(\boldsymbol{u}) (\boldsymbol{u} \times (-\nabla_{\boldsymbol{u}} V(\boldsymbol{u}))) \tag{A.10}$$

where $\rho_{\mathcal{A}}$ is the density distribution of the asteroid and $\mathcal{A}$ indicates the volume of the asteroid. Making use of one more

identity concerning the derivatives of spherical harmonics:

$$\begin{aligned}\boldsymbol{u}\times\nabla R_{\ell m}(\boldsymbol{u}) =& \frac{1}{2}\Big[(i\hat{\boldsymbol{x}}-\hat{\boldsymbol{y}})(\ell-m+1)R_{\ell,m-1}(\boldsymbol{u}) \\ &+(i\hat{\boldsymbol{x}}+\hat{\boldsymbol{y}})(\ell+m+1)R_{\ell,m+1}(\boldsymbol{u}) \\ &+2im\hat{\boldsymbol{z}}R_{\ell m}(\boldsymbol{u})\Big],\end{aligned} \tag{A.11}$$

tidal torque can now be expressed as a function only of the constants $J_{\ell m}$, $K_{\ell m}$, $a_{\mathcal{A}/\mathcal{B}}$, $I_{\mathcal{A}/\mathcal{B}}$, and the asteroid orientation and position (equation 4). Some $K_{\ell m}$ terms are written in this equation with $|m|>\ell$; these should all be taken to be zero.

A.4 Equations of motion

The equations of motion of the asteroid position $\boldsymbol{D}$ are given by Newton's law of gravitation

$$\dot{\boldsymbol{V}} = -\frac{G\mu_{\mathcal{B}}}{D^3}\boldsymbol{D} \qquad \dot{\boldsymbol{D}} = \boldsymbol{V} \tag{A.12}$$

where $\boldsymbol{V}$ is the asteroid velocity in the inertial frame. Rather than derive equations of motion for the Euler angles (which suffer from gimbal lock), we instead represent the orientation of the asteroid with a quaternion $\widetilde{\boldsymbol{q}}$ which can be converted into Euler angles to compute $\mathcal{D}(\alpha,\beta,\gamma)$. This quaternion evolves as

$$\dot{\widetilde{\boldsymbol{q}}} = \frac{1}{2}\widetilde{\boldsymbol{q}}\widetilde{\boldsymbol{\omega}}. \tag{A.13}$$

for angular velocity $\boldsymbol{\omega}$ given in the body-fixed frame. The equations of motion of $\boldsymbol{\omega}$ in turn are given by

$$\begin{aligned} I_x\dot{\omega}_x - \omega_y\omega_z(I_y-I_z) &= \tau_x \\ I_y\dot{\omega}_y - \omega_z\omega_x(I_z-I_x) &= \tau_y \\ I_z\dot{\omega}_z - \omega_x\omega_y(I_x-I_y) &= \tau_z. \end{aligned} \tag{A.14}$$

Equations 4, 5, A.12, and A.14 form a set of non-linear, first-order coupled differential equations in which can be numerically integrated. They are expressed in terms of the physical parameters $I_{\mathcal{A}/\mathcal{B}}$, $a_{\mathcal{A}/\mathcal{B}}$, $J_{\ell m}$, and $K_{\ell m}$ which are constant if the asteroid is rigid and the central body does not rotate.

APPENDIX B: COMPARING ORIENTATION & ANGULAR VELOCITY DATA

To extract the density distribution of an asteroid, the main text assumes that the angular velocity data of the asteroid is observable. It is possible that the orientation of the asteroid may be more readily available as a data set, notably if a large collection of radar antenna fail to follow the encounter sufficiently. In this appendix, we generate an orientation data set for the reference asteroid flyby, extract density moments from it, and compare the results to moments extracted from angular velocity data.

B.1 Uncertainty model

To use an asteroid orientation data set rather than angular velocity, we must create an uncertainty model for orientation observations and produce a likelihood to be used by the MCMC (replacing equation 7).

For the sake of this appendix, we will assume that all observations of orientation $\widetilde{\boldsymbol{q}}$ differ from the true orientation $\widetilde{\boldsymbol{q}}^*$ by a rotation by some angle ϕ around an axis drawn from a uniform distribution on the unit sphere, where ϕ is drawn from a normal distribution with mean zero and standard deviation σ_ϕ. As in the rest of the paper, orientation is expressed as a quaternion $\widetilde{\boldsymbol{q}} = q_r + q_i\boldsymbol{i} + q_j\boldsymbol{j} + q_k\boldsymbol{k}$. The angle ϕ can be extracted from these quaternion components to yield a likelihood of

$$\ln\mathcal{L} = -\frac{2}{\sigma_\phi^2}\sum_i\left(\cos^{-1}\left|\left[\widetilde{\boldsymbol{q}}_i(\widetilde{\boldsymbol{q}}_i^*)^{-1}\right]_r\right|\right)^2 \tag{B.1}$$

where a subscript i denotes the ith element of the data set. It is assumed that both quaternions have norm one.

B.2 Moment uncertainty comparison

With the likelihood defined, we generate both angular velocity and orientation data for the asymmetric reference asteroid configuration and extract density moment PPDs for both data sets via the fit method defined in the main text. Due to the different uncertainty models used for the orientation and angular velocity data sets, this set-up does not allow direct comparison between the amount of moment uncertainty for both data sets. (If one data set yields more precise moments than the other, one could not determine whether the effect is due to increased observational precision in the data set or the use of a data type that better constrains density moments.) However, the relative uncertainty of moments can be compared.

To make this comparison, we compute moment uncertainties $\sigma(K_{\ell m})$ for both data sets. We then scale the moment uncertainties attained from the angular velocity data set so that the average $\sigma(K_{\ell m})$ value is equal to that of the orientation data set. This is equivalent to choosing observational uncertainties for the angular velocity data set which yield density moments to the same precision as the observational data set. The resulting PPDs for the density moments of both data sets are displayed in figure B.1 relative to the true values.

The figure demonstrates that using orientation data rather than angular velocity data does not greatly affect the relative uncertainties of density moments, except in the case of γ_0, which is much more precisely constrained by orientation data than by angular velocity data. This result is expected due to the following argument. If the initial orientation of the asteroid is known, then the orientation of the next data point can be determined by knowledge of the asteroid's angular velocity at that moment. Thus, an orientation data set can be produced from an angular velocity data set and vice versa given an initial asteroid orientation. That initial orientation is defined up to γ_0 by the assumption of no initial tumbling, so we expect the angular velocity data set to yield increased uncertainties in γ_0 only, relative to the observational data, to a first approximation.

A smaller effect observed in figure B.1 is that the orientation data set yields similar uncertainties for all density moments of fixed ℓ, whereas the angular velocity data set tends to yield larger uncertainties for small $|m|$. However, this has little effect on the density distributions extracted by the finite element model (not shown); the average density uncertainty $\langle\sigma_\rho/\rho\rangle$ are essentially equivalent between the two data sets, as is the extracted distribution of density and density uncertainty.

APPENDIX C: ADDITIONAL DENSITY DISTRIBUTION MODELS

Two models were discussed in section 2.4 to translate density moment constraints into density distribution constraints. Here we outline two additional models which are less conventional but still useable for extracting density distribution properties.

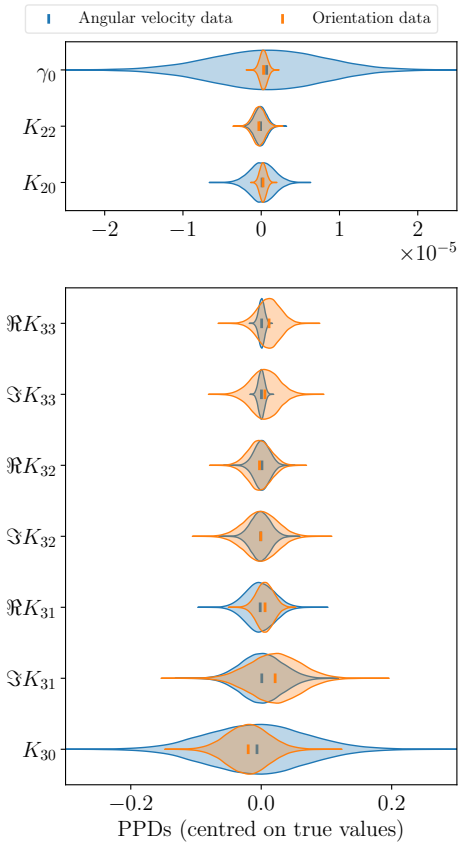

Figure B.1: PPDs for each parameter as extracted from angular velocity (blue) and orientation (orange) data. First order parameters are shown in the top panel and second-order parameters in the bottom. Mean values are also shown as vertical lines. Both data sets produce similar constraints on parameters, except in the case of γ_0.

Unlike the finite element and lumpy models discussed in the main text, these models will yield smooth distributions with no discrete transitions.

C.1 Nearly-uniform model

In this "nearly-uniform" model, we pick one density distribution from the many distributions consistent with the data by maximizing a prior distribution $f[\rho(\boldsymbol{r})]$. Any prior distribution can be chosen, but the following prior is both interesting and numerically efficient.

As part of our prior, we require that the asteroid density distribution satisfy $I_{\mathcal{A}} = \mu_{\mathcal{A}} a_{\mathcal{A}}^2$. This constraint is desirable as it is obeyed for uniform density distributions. To define the prior, we divide the asteroid into $n \gg 1$ small regions of volume V, each with position $\boldsymbol{r}_i$ and density $\rho_i = \delta_i + 1$. Setting the mass of the asteroid equal to its volume, the average density is 1, so δ_i is the difference between the average and local density. We set $f[\rho(\boldsymbol{r})]$ to be a multivariate-Gaussian distribution on δ_i, centred on zero to minimize non-uniformity, i.e.

$$f[\rho(\boldsymbol{r})] \propto \prod_i \exp\left(-\frac{\delta_i^2}{2\sigma^2}\right) \implies \ln f[\rho(\boldsymbol{r})] \simeq -\sum_i \delta_i^2 \quad \text{(C.1)}$$

where σ is an irrelevant constant. The density moments, MOI scale, and mass are

$$K_{\ell m} = \frac{V}{\mu_{\mathcal{A}} a_{\mathcal{A}}^{\ell}} \sum_i (\delta_i + 1) R_{\ell m}(\boldsymbol{r}_i) \quad \text{(C.2)}$$

$$I_{\mathcal{A}} = \mu_{\mathcal{A}} a_{\mathcal{A}}^2 = V \sum_i (\delta_i + 1) r_i^2 \quad \text{(C.3)}$$

$$\mu_{\mathcal{A}} = V \sum_i (\delta_i + 1) \implies 0 = \sum_i \delta_i. \quad \text{(C.4)}$$

Writing δ_i as an n-dimensional vector $\boldsymbol{\delta}$, equation C.2 is a matrix equation for $K_{\ell m}$, and equations C.3 and C.4 are vector dot product equations. Combining $K_{\ell m}$, $I_{\mathcal{A}}$, and 0 into a single vector $\boldsymbol{K}$, these equations can be written as a single underdetermined matrix equation we denote as

$$\boldsymbol{K} = M\boldsymbol{\delta} + \boldsymbol{C}, \quad \text{(C.5)}$$

where the components of constant matrix M and constant vector $\boldsymbol{C}$ are known given a fixed layout of the n regions. Some of the components of $\boldsymbol{K}$, such as $I_{\mathcal{A}}$, $\mu_{\mathcal{A}}$, and K_{1m}, are constraints. We treat the other components as parameters of the model. The task is then to find $\boldsymbol{\delta}$ that satisfies equation C.5 and maximizes $f(\boldsymbol{\delta})$. But the form of equation C.1 shows that the maximum of $\ln f$ (also the maximum of f) is the minimum of $|\boldsymbol{\delta}|^2$. This shortest value of $\boldsymbol{\delta}$ that obeys equation C.5 is given by the Moore-Penrose inverse:

$$\boldsymbol{\delta} = M^+(\boldsymbol{K} - \boldsymbol{C}); \qquad M^+ = M^\dagger (M M^\dagger)^{-1} \quad \text{(C.6)}$$

where $M^\dagger$ is the hermitian conjugate of M.

The prior distribution on $\rho(\boldsymbol{r})$ discussed in section 2.3 can be implemented by individually checking the components $\boldsymbol{\delta}$ computed by equation C.6 and confirming that $1 + \delta_i$ lies within the acceptable range of densities.

C.2 Harmonic model

In the "harmonic model", we limit ourselves to density distributions that are harmonic; i.e., they satisfy $\nabla^2 \rho(\boldsymbol{r}) = 0$. We have no physical justification for why this assumption should be true, but it is useful as a simplification to gain qualitative insight into the properties of the asteroid density distribution.

A harmonic density distribution can be expanded in terms of the spherical harmonics as $\rho(\boldsymbol{r}) = \sum_{\ell m} C_{\ell m} R_{\ell m}(\boldsymbol{r})^*$ where $C_{\ell m}$ are complex, free parameters. This series can be truncated at some maximum ℓ. The density moments, MOI scale, and mass can then be explicitly computed as a function of $C_{\ell m}$:

$$K_{\ell m} = \frac{a_{\mathcal{A}}^{2-\ell}}{I_{\mathcal{A}}} \sum_{\ell m} C_{\ell' m'} \int_{\mathcal{A}} d^3 r R_{\ell' m'}(\boldsymbol{r})^* R_{\ell m}(\boldsymbol{r}) \quad \text{(C.7)}$$

$$I_{\mathcal{A}} = \sum_{\ell m} C_{\ell m} \int_{\mathcal{A}} d^3 r R_{\ell m}(\boldsymbol{r})^* r^2 \quad \text{(C.8)}$$

$$\mu_{\mathcal{A}} = \sum_{\ell m} C_{\ell m} \int_{\mathcal{A}} d^3 r R_{\ell m}(\boldsymbol{r})^*. \quad \text{(C.9)}$$

Since the integrals are independent of the parameters, they can be computed before solving for $C_{\ell m}$. Furthermore, their values when $\mathcal{A}$ is spherical gives us insight into the influence of $K_{\ell m}$ on density distributions. In this case, $I_{\mathcal{A}} \propto C_{00}$ and the integral of equation C.7 is non-zero only when $\ell' = \ell$ and $m' = m$. Therefore, $C_{\ell m}$ is proportional to $K_{\ell m}$. The density distribution can be immediately visualized given the density moments as a sum of the solid spherical harmonics $R_{\ell m}$ weighted by $K_{\ell m}$.

When the asteroid is non-spherical, the shape itself contributes to $K_{\ell m}$ so as to alter this picture.

$C_{\ell m}$ can be treated as parameters for a fitting method (such as an MCMC) that enforces our bounds on $\rho(\boldsymbol{r})$. With the integrals pre-computed, obtaining $K_{\ell m}$ from $C_{\ell m}$ is fast. We impose these bounds by acknowledging that harmonic functions such as $\rho(\boldsymbol{r})$ in a region such as $\mathcal{A}$ attain their maxima on the boundary of the region, so that it is only necessary to ensure that ρ lies within the allowed range on the asteroid boundary rather than within the entire asteroid. This can be done by parametrizing the asteroid surface as a function of two variables (e.g., latitude and longitude) and minimizing and maximizing ρ with respect to those variables, ensuring these minima and maxima are within the allowed range.